Morphological development of multilamellar phospholipid film depending on drying kinetics

M. Hishida,[1,*] N. L. Yamada,[2] K. Yoshikawa,[1] and H. Seto[2]
[1]*Department of Physics, Graduate School of Science, Kyoto University, Kyoto 606-8502, Japan*
[2]*High Energy Accelerator Research Organization, Tsukuba 305-0801, Japan*
(Received 6 June 2009; revised manuscript received 9 October 2009; published 30 November 2009)

The mechanism for the formation of solid-supported phospholipid membranes during a drying process was investigated. Terracelike multilamellar structures were found to develop from a micellar solution with either spinodal decompositionlike process or nucleation growth, depending on the evaporation rate of an organic solvent. In contrast to the well-known kinetics of phase separation, fast drying induces nucleation while slow drying induces spinodal decompositionlike lipid-film formation. The existing models for the interpretation of phase separation are not sufficient to understand this unexpected kinetics. We suggest a schematic model with which this kinetic feature can be interpreted in terms of a self-assembly pathway in a three-component phase diagram for a phospholipid, organic solvent, and water.

DOI: 10.1103/PhysRevE.80.051407 PACS number(s): 82.70.Uv, 64.70.fm, 81.16.Dn, 87.14.Cc

I. INTRODUCTION

Phospholipid bilayers have attracted considerable interest from the viewpoints of biology, chemistry, and physics as simple models of biomembranes. In particular, solid-supported lipid bilayers have recently been the subject of active studies for better understanding of membrane adhesion on a solid, the biofunctionality of immobilized biomembranes, self-assembled micropatterned-substrates, etc. [1–3]. Solid-supported lipid bilayers are also used for vesicle formation, where giant vesicles larger than 1 μm in diameter are effectively formed by the hydration of multistacked lipid bilayers on a solid substrate [4–8].

Solid-supported phospholipid bilayers are often prepared by evaporating organic solvent from a solution of lipid and organic solvent on a substrate. It has been shown that a μm-scale terracelike morphology of dried multistacked phospholipid bilayers is formed by evaporation when the lipid is in a liquid-crystalline L_α phase [3,6,9]. This terracelike morphology is crucial for the formation of giant lipid vesicles, since this morphology dominates the kinetics in the hydration of lipids and the efficiency of vesicle formation [6,7]. These results suggest that a deeper understanding of the mechanism for the generation of lipid bilayers on a substrate during the drying process is essential for obtaining desired giant vesicles in an effective manner.

The self-assembled structures of amphiphilic molecules often depend on nonequilibrium formation kinetics due to complex free-energy landscapes with a large number of degrees of freedom [10,11]. In general, the kinetic process of the self-assembly of an ordered structure can be classified as one of two different mechanisms: nucleation growth or spinodal decomposition. The nucleation/spinodal kinetics depend on the quench depth of a control parameter such as temperature; a deep quench induces spinodal decomposition while a shallow quench results in nucleation growth as discussed by the Cahn-Hilliard model [12,13]. The mechanism of the formation of a lipid film is also considered to depend on the kinetics of self-assembly under drying. Thus, to clarify the mechanism of self-assembly, we must first understand the dependence of lipid-film morphology on the drying kinetics. Although there has been growing interest in the kinetics of the self-assembly of amphiphilic molecules [7,10,11,14,15], a basic understanding has not yet been established.

In the present study, we investigated the mechanism of the formation of a lipid dry film under the evaporation of organic solvents, with special focus on the kinetics of self-assembly with changes in the evaporation rate. By using phase-contrast microscopy and time-resolved small-angle x-ray scattering (TR-SAXS), we performed *in situ* observations of the kinetics of lipid-film formation under a drying process. The results suggest that slower evaporation induces a specific feature on lamellar formation similar to the kinetics of spinodal decomposition, in contrast to the well-known kinetics of phase separation.

II. MATERIALS AND METHODS

1,2-Dioleoyl-sn-glycero-3-phosphocholine in powder form (DOPC, purchased from Wako Chemical Inc.) was used as a phospholipid without further purification. Since DOPC is in the liquid-crystalline phase at room temperature, the dry film tends to exhibit a terracelike morphology [6]. Chloroform (99% from Nacalai Tesque, Inc.) and *n*-octane (98% from Nacalai Tesque, Inc.) were used as organic solvents without further purification. The relative evaporation rates of *n*-octane and chloroform against butyl acetate are 1.4 and 11.6, respectively (boiling points are 126 and 62 °C, respectively) [16]. For the experiments, DOPC was dissolved in these organic solvents to give a concentration of 50 mM.

Measurements by phase-contrast microscopy were performed using an inverted microscope (TE300, Nikon). 5 μL of the solution was deposited on a slide glass and exposed to air at room temperature (22 ± 2 °C) and at a relative humidity of 50%–65%. Only the organic solvent evaporated gradually, and several hundreds of lipid bilayers were stacked on the substrate in this condition.

*Present address: Institute for Integrated Cell-Material Sciences, Kyoto University, Kyoto 606-8501, Japan; hishida@scphys.kyoto-u.ac.jp

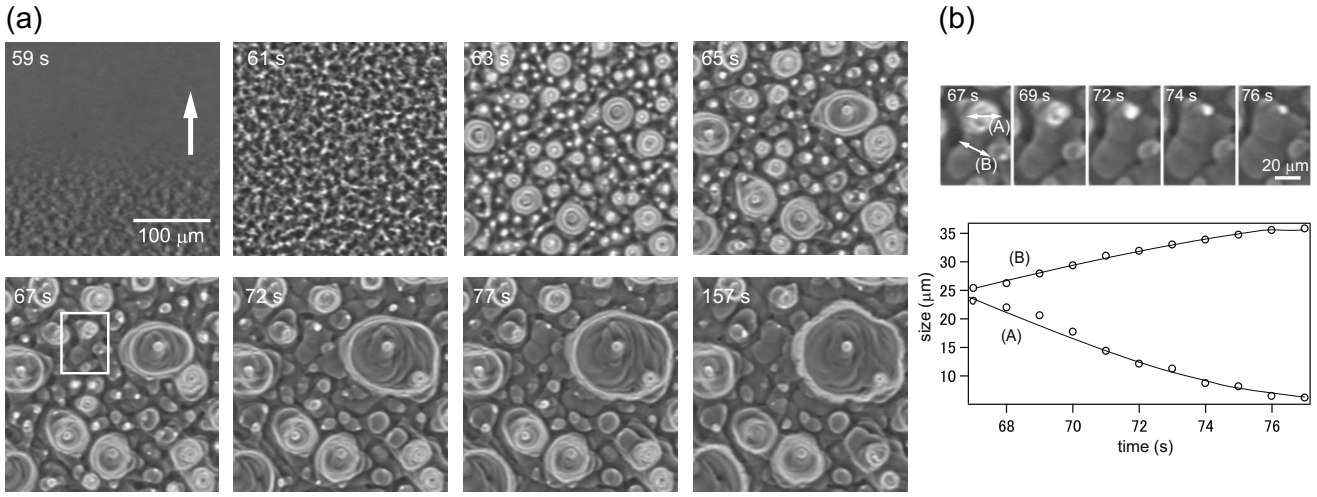

FIG. 1. (a) Time-series images of lipid-film formation under the evaporation of chloroform as observed by phase-contrast microscopy. At about 59–60 s after the deposition of solution, bulk solvent evaporates and the interface moves upward from the bottom (white arrow). The nuclei of terracelike lamellar structures grow from the disordered lipid film. (b) Upper images show typical Ostwald ripening in the framed rectangle at 67 s in (a). Time variations in the sizes of small (A) and large (B) terraces are depicted in the lower graph. A relatively small terrace structure shrinks as it is absorbed into a larger one.

TR-SAXS experiments were carried out at BL40B2, SPring-8, JASRI (Japan Synchrotron Radiation Research Institute), Japan. The wavelength and beam diameter of the x-ray were 0.8 Å and 0.4 mm, respectively. The beam diameter was much larger than the total thickness of the lipid film (<10 μm). The scattered x-ray beam was detected by CCD (C4880–10, Hamamatsu). The exposure time for each time-resolved measurement was 1 s with 0.6 s intervals, and TR-SAXS measurements were started at about 30 s after the deposition of solution. The outer surface of a glass rod (2 mm diameter) was used as a substrate to obtain a wide range of diffraction angles, as in our previous study [7]. 10 μL of solution was deposited on the rod so as to obtain almost the same thickness of lipid dry film as in the microscopy measurement. The temperature and humidity were essentially the same as in the measurements by optical microscopy.

III. RESULTS AND DISCUSSION

The results of evaporation-induced lipid-film formation as observed by phase-contrast microscopy with chloroform as the organic solvent are shown in Fig. 1. Time 0 s indicates when the chloroform solution of 50 mM DOPC was deposited on the substrate. The measured area was near the center of a droplet. At about 59 s after deposition, the bulk chloroform evaporated and the lipid film remained on the substrate. At this stage, the lipid film had some fluidity, which suggests that chloroform still remained in the film.

After the chloroform in the bulk solvent had evaporated, the residual lipid film developed into a large terracelike morphology of lamellae, which required 1 min or longer. Soon after the bulk solvent had evaporated, lipid film with a rough surface appeared at 61 s. Later, terracelike lamellar structures emerged in the disordered film, which showed the kinetic characteristics of nucleation and growth (63–65 s). Relatively large islands of the terrace morphology then grew, while small islands shrunk, as shown in Fig. 1(b). Such time-dependent changes in morphology can be interpreted in terms of Ostwald ripening [17,18]. Finally, after 150 s, the terracelike morphology appeared to be stable, and the size of the terrace remained almost constant thereafter.

Figure 2(a) exemplifies the process of lipid-film formation with a slower rate of solvent evaporation achieved by partial shielding of the sample vessel, where the evaporation rate of chloroform was 2–3 times slower than that without shielding as in the case of Fig. 1. At 117 s, the process of film formation started and the growth kinetics of lamellae proceeded until around 430 s. The growth kinetics of a terracelike morphology in this case is apparently different from those in open air (Fig. 1): the growth of lamellae under slow drying proceeds as in spinodal decompositionlike kinetics. Soon after the bulk solvent had evaporated, rather small domains appeared homogeneously over the observed area and became distinct at 120–350 s. The existence of a characteristic fastest-growing length scale is a typical feature of the early stage of spinodal decomposition. At about 350 s, the terrace morphology started to grow, and this growth continued until around 430 s. This process corresponds to the later stage of spinodal decomposition known as coarsening. After 430 s, the morphology tended to show almost no change.

Figures 2(b) and 2(c) show the 1D power spectrum $J(k)$ of the microscopy images analyzed by Fourier transformation and the time variation in the characteristic size of the terracelike morphology D evaluated from the peak position ($D=2\pi/k$), respectively. At 120–350 s, the size is almost constant at about 13 μm, and thereafter the size increases monotonically until 430 s. The peak intensity of the spectrum increases between 120–200 s, which indicates that the multilamellar structure with a characteristic size becomes clear in this stage. A Fourier transformation analysis confirmed that the kinetics exhibited spinodal decompositionlike behavior.

In Fig. 3, lipid-film formation in the slow drying process is shown for *n*-octane as the organic solvent. The evaporation

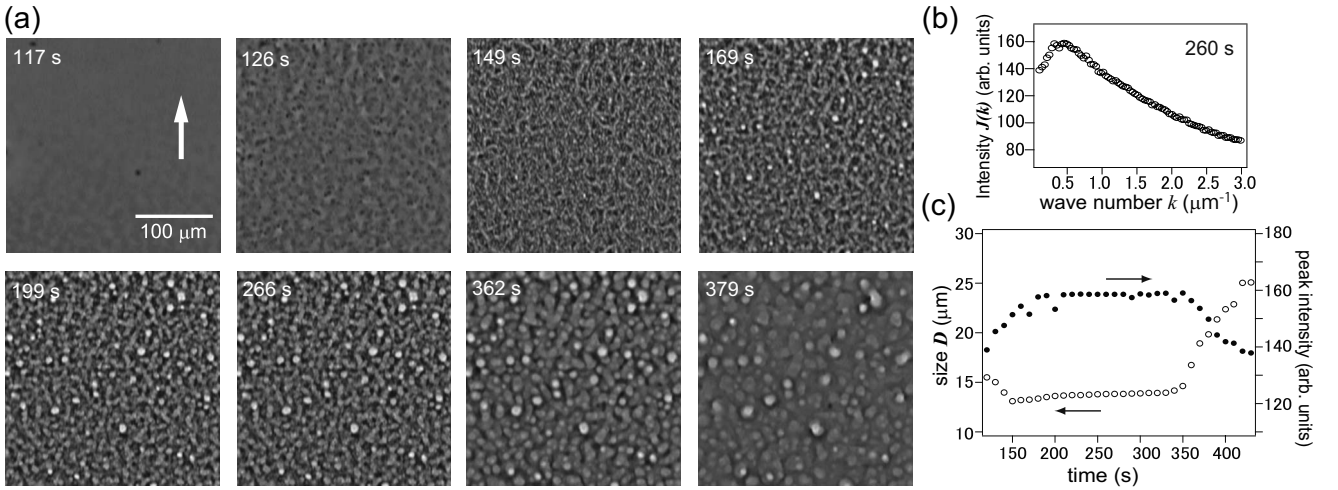

FIG. 2. (a) Lipid-film formation under the slow evaporation of chloroform by shielding the solution. The formation kinetics of a terracelike lamellar structure proceeded as in spinodal decompositionlike behavior. (b) 1D power spectrum $J(k)$ obtained by fast Fourier transform analysis of the image at 260 s. A peak at 0.5 μm^{-1} corresponds to the characteristic size of the terrace morphology $D=2\pi/k$. (c) The characteristic size D of the terracelike morphology (open circle) and the peak intensity (closed circle) of the power spectrum at each time point.

rate of *n*-octane is eight times slower than that of chloroform in open air. In this case, spinodal decompositionlike kinetics was observed in the formation of a terracelike lamellar structure, as in the case of the slow evaporation of chloroform with shielding. After the bulk solvent had evaporated at 400 s, a terracelike morphology with a typical size of about 12 μm became clear between 400 and 600 s, and the terracelike morphology of lamellae grew until 1500 s. The results of these experiments suggest that the kinetics of lipid-film formation depend not on the species of solvent, but rather on the evaporation rate: fast evaporation induces nucleation growth, while slow evaporation induces the spinodal decompositionlike formation of a terracelike lamellar structure.

As mentioned in the introduction section, spinodal decomposition and nucleation growth processes are understood in terms of phase-separation kinetics [12,13], and it is well-known that a deep quench induces spinodal decomposition. In our case, the evaporation rate of the organic solvent corresponds to the quench depth. However, fast evaporation of the organic solvent, corresponding to a deep quench, results in the nucleation growth of a lamellar structure.

To clarify the molecular origin of this discrepancy in the kinetics, the pathway of the self-assembly of lipids in the drying process in nm-scale was investigated by TR-SAXS measurements under the same conditions as in the microscopy measurements. Figure 4 shows TR-SAXS profiles during the drying process of the DOPC/*n*-octane solution. As shown in Fig. 4(a), two-dimensional profiles of SAXS changed from a nonoriented homogeneous pattern to a vertically oriented pattern, i.e., lamellar parallel to the substrate, around 400 s after deposition of the solution. This result indicates that the homogeneous dispersion of some self-assembled structure exhibited a transition to the lamellar structure on the substrate at around 400 s.

In Fig. 4(b), one-dimensional scattering profiles $I(q)$ before 400 s are shown for a more detail analysis (azimuthal averaging was done for only 30° around the upper area of the scattering profiles). To analyze the structure of lipid assembly in this process, functional fitting was carried out for the profiles using

$$I(q) = I_{\mathrm{mic}}(q) + I_{\mathrm{lam}}(q). \tag{1}$$

$I_{\mathrm{mic}}(q)$ is the scattering function for the homogeneous dispersion of micelles in the solution before film formation, which is given by

$$I_{\mathrm{mic}}(q) \propto |F_{\mathrm{mic}}(q)|^2 S_{\mathrm{mic}}(q). \tag{2}$$

For the form factor $F_{\mathrm{mic}}(q)$, a cylinder model [19]

$$|F_{\mathrm{mic}}(q)|^2 \propto \int_0^{\pi/2} \left| \frac{\sin\left(q\frac{H}{2}\cos\alpha\right) J_1(qR\sin\alpha)}{q^2 \sin\alpha\cos\alpha} \right|^2 \sin\alpha d\alpha \tag{3}$$

was found to fit the results well, where R is the radius of a cylinder, H is the length of a cylinder with a Schulz distribution, and J_1 is the first-order Bessel function. As the struc

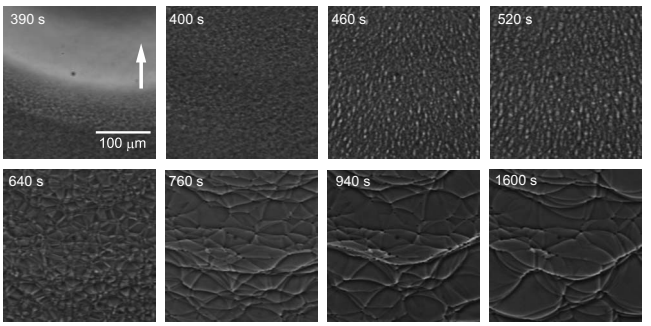

FIG. 3. Lipid-film formation under the evaporation of *n*-octane. The spinodal decompositionlike formation of a terracelike morphology of lamellae is exhibited.

ture factor, $S_{\mathrm{mic}}(q)$, a hard-sphere model [19–21],

$$S_{\mathrm{mic}}(q) = \frac{1}{1 + 24\eta G(2R_{\mathrm{mic}}q)/(2R_{\mathrm{mic}}q)} \tag{4}$$

$$G(A) = \frac{\alpha(\sin A - A\cos A)}{A^2} + \frac{\beta(2A\sin A + (2 - A^2)\cos A - 2)}{A^3} + \frac{\gamma[-A^4\cos A + 4\{(3A^2 - 6)\cos A + (A^3 - 6A)\sin A + 6\}]}{A^5} \tag{5}$$

$$\alpha = \frac{(1 + 2\eta)^2}{(1 - \eta)^4} \tag{6}$$

$$\beta = \frac{-6\eta(1 + \eta/2)^2}{(1 - \eta)^4} \tag{7}$$

$$\gamma = \frac{\eta\alpha}{2}, \tag{8}$$

was approximately used for concentrated cylinders, where the volume fraction of micelles η and the size of micelles R_{mic} are the fitting parameters. $I_{\mathrm{lam}}(q)$ is the scattering function of lamellae, for which only Lorentzian function is applied as the structure factor for a Bragg peak so as not to increase fitting parameters.

By the fitting procedure, the change in the structure of lipid self-assembly at the earlier stage before film formation can be summarized as follows. First, DOPC molecules in *n*-octane formed cylinderlike inverted micelles at 50 mM. The length and radius of the cylinders were evaluated to be a hundred to several thousands of angstroms (with a very broad distribution) and about 20 Å, respectively. In the drying process, the inverted cylindrical micelles were concentrated, and the correlation between micelles became significant as a broad peak at $q \approx 0.09$ Å^{-1} after 350 s. The concentrated inverted cylindrical micelles showed a kinematical transition to a lamellar phase oriented to the substrate at around 400 s, which is reflected by a Bragg peak at $q = 0.125$ Å^{-1} that corresponds to a lamellar repeat distance of 50 Å. Time dependence of the effective volume fraction of lipid micelles evaluated from the fitting parameter η in $S_{\mathrm{mic}}(q)$ is shown in Fig. 4(c) ($\eta = 0.033$ at 43 s is consistent with the initial concentration of DOPC in *n*-octane, i.e., 50 mM corresponds to $\eta \sim 0.03$). The result indicates that the inverted cylindrical micelles had a transition to the lamellae at around $\eta = 0.4–0.5$. After the formation of the lamellae on the substrate, the peak intensity increased and the peak position shifted to a higher-q region between 400–4900 s, as shown in Fig. 4(d). This result indicates that *n*-octane remained between bilayers in this time region even when the growth of the terrace morphology stopped after 1500 s, since the evaporation of solvent in between bilayers results in a decrease in the repeat distance. At 4900 s, the lamellar repeat distance reached about 45.9 Å ($q = 0.137$ Å^{-1}), which is consistent with that of fully dried DOPC film [22]. The result indicates *n*-octane evaporated entirely at this time. Essentially the same process for the self-assembly of DOPC was observed under the evaporation of chloroform.

No other scattering profile, such as a signal corresponding to the hexagonal packing of inverted cylindrical micelles, was observed during the processes under these experimental conditions, i.e., at room temperature and at a relative humidity of 50%–65%. On the other hand, an intermediate mesh phase, i.e., the lamellarlike structure with intralamellae pores as reported in phospholipid or other surfactant systems [23–26], was observed even at room temperature when TR-SAXS measurements were performed under less humid conditions for both solvents. For example, Fig. 5 shows the scattering profile of the lipid film after the evaporation of *n*-octane at relative humidity $<50\%$. The structure was found to be rhombohedral by referring the reciprocal lattice as shown in Fig. 5, which is consistent with the results of the structure of dried DOPC at 25 °C and at 35% relative humidity [23]. The lipid film in the intermediate mesh phase was observed as a disordered morphology by phase-contrast microscopy. These results suggest that the solution of lipids and organic solvent absorbs water molecules depending on the humidity of the surrounding atmosphere, and the amount of water in the system dominates the pathway of self-assembly under drying. Thus, the experimental trends can be explained schematically by referring to a typical phase diagram of an amphiphile with water and oil, as shown in Fig. 6; the intermediate mesh phase is formed by evaporation at low humidity (path C in Fig. 6), whereas the lamellar phase appears at high humidity (paths A and B).

If we consider the pathway in the phase diagram, the two kinetics of lamellae formation observed by microscopy can be interpreted as follows. When evaporation is slow enough, the system undergoes phase separation as in path A, which can be approximately discussed by a conservative time-dependent Ginzburg-Landau (TDGL) equation (Cahn-Hilliard equation). In the microscopy experiment, spinodal decomposition between micelles (dark area in the microscopy images) and lamellae (light area that grows to a terrace-like morphology) are observed as phase-separation kinetics that took 100–200 s. On the other hand, when the rate is much faster than the phase-separation kinetics, the system comes into the lamellar phase before undergoing phase separation (path B). Therefore, nucleation growth takes place as in a normal phase transition or crystal growth, as described by a nonconservative TDGL equation.

Another model can be considered to understand the nucleation-spinodal dilemma. Muthukumar proposed that

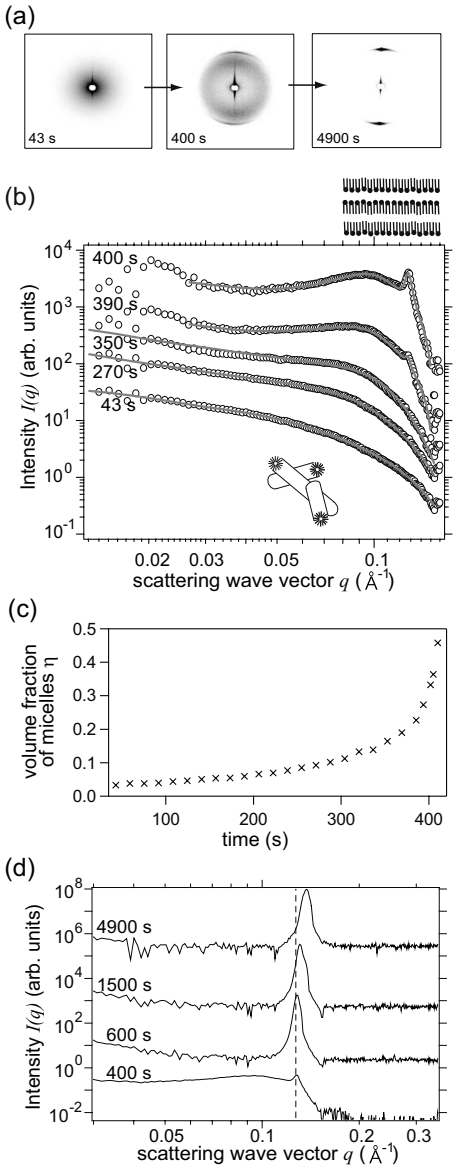

FIG. 4. TR-SAXS profiles of DOPC/*n*-octane under drying. (a) The change in two-dimensional SAXS profiles. (b) One-dimensional SAXS profiles during 40–400 s after the deposition of solution. The solid lines indicate the results of functional fitting using Eq. (1). (c) Time dependence of the effective volume fraction of lipid micelles η obtained by the functional fitting with Eq. (1). (d) One-dimensional SAXS profiles during 400–4900 s. The dashed line is the guide of the peak position at 400 s (about 0.125 $Å^{-1}$).

"baby nuclei" are formed in the early stage of the spinodal-like crystallization of polymers [27]. In this case, the observed spinodal-like behavior is not true spinodal decomposition, which is described by the Cahn-Hilliard approach, but rather is due to the late-stage coarsening of nucleation growth, where the peak obtained by Fourier transformation [such as in Fig. 2(b)] is attributed to the correlation between semicrystalline periodicity. The baby nuclei scenario has been confirmed by an experiment of polymer crystallization [29]. In the same way, the observed spinodal-like lipid-film formation cannot be true spinodal decomposition, and the kinetics of lipid-film formation with both fast and slow drying can be interpreted only by nucleation growth kinetics.

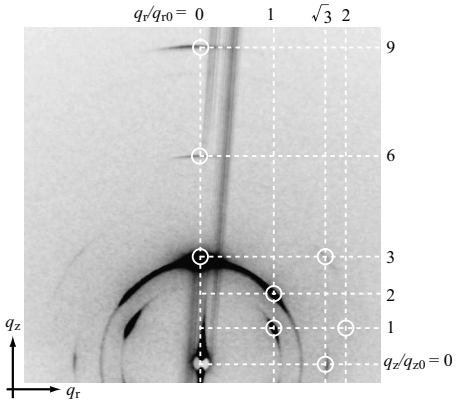

FIG. 5. Upper-half plane of two-dimensional SAXS profile of DOPC dry film formed with drying *n*-octane under a humidity of less than 50%. The dashed lines are the guide at $q_z/q_{z0}=0,1,2,3,6,9$ and $q_r/q_{r0}=0,1,\sqrt{3},2(q_r=\sqrt{q_x^2+q_y^2})$. The observed scattering peaks (white circles) are coincident with the reciprocal lattice of the rhombohedral symmetry (Ref. [24]).

To distinguish whether the mechanism is nucleation or spinodal decomposition, a simple model has been proposed in the literature [27], where the growth rate of the power intensity during crystallization is a good criterion. In terms of the Cahn-Hilliard model, the generalized form of the power spectrum intensity with respect to wave number k and time t, $J(k,t)$, is calculated as,

$$J(k,t) = J(k,0)\exp[2\Omega(k)t], \tag{9}$$

where $\Omega(k)$ is the growth rate of the intensity given by,

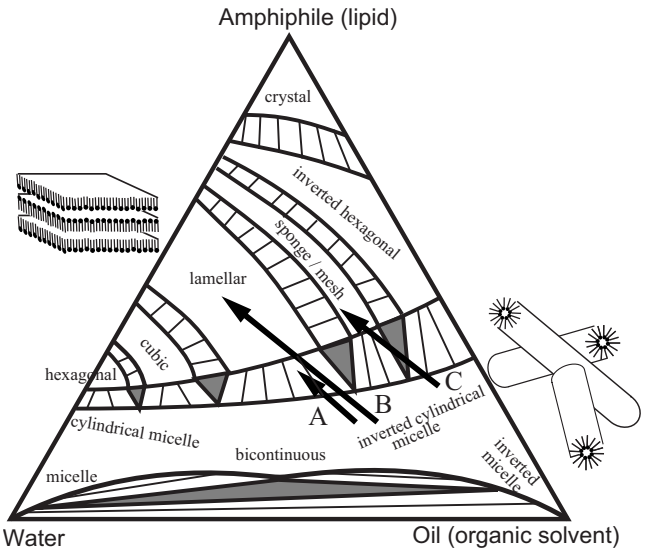

FIG. 6. Schematic view of the self-assembly of lipid in the drying process with a typical phase diagram of an amphiphile (lipid), oil (organic solvent), and water system (Ref. [10]). Depending on the evaporation rate, the pathway of self-assembly from micelles to a lamellar phase divides into path A or B. When the water content is low, a sponge or an intermediate mesh structure appears under drying (path C).

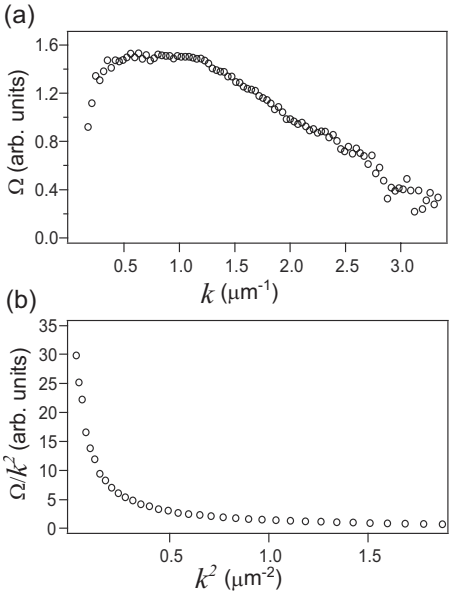

FIG. 7. (a) The growth rate of the power intensity Ω with respect to wave number k, which is obtained from the microscopic image of drying DOPC/*n*-octane (Fig. 3) at 600 s by using Eq. (9). (b) The Cahn-Hilliard plot, Ω/k^2 with k^2.

$$\Omega(k) = -Mk^2\left(\frac{\partial^2 G}{\partial \phi^2} + 2\kappa k^2\right). \tag{10}$$

M is the mobility term, G is the Gibbs free energy, and κ is the gradient energy coefficient. Therefore, Ω/k^2 plotted with respect to k^2 shows a negative linear slope, which is the evidence for spinodal decomposition. Muthukumar proposed that when nucleation takes place in the early stage of spinodal-like crystallization as baby nuclei, the growth rate Ω becomes

$$\Omega \sim k^2\left(\Delta T - k^2 - \frac{1}{k^2}\right). \tag{11}$$

In this case, Ω/k^2 rises sharply with k^2 at a small k region [27,28].

Figure 7(a) shows the growth rate of the power spectrum Ω during lipid-film formation, which is derived by Fourier transformation and using Eq. (9) for the microscopy image in Fig. 3 at 600 s. Ω/k^2 is plotted with respect to k^2 in Fig. 7(b). In the case of lipid-film formation with slow drying, Ω/k^2 decreases drastically with respect to k^2. A similar behavior of Ω/k^2 has been reported in the literature [30]. The positive growth rate Ω at $0<k<k_c$ (where k_c is the critical wave number) suggests that the observed behavior is somewhat analogous to spinodal decomposition derived from the Cahn-Hilliard model, rather than nucleation growth. However, the behavior of the obtained Ω/k^2 does not correspond to any existing scenario, such as the model of early-stage nucleation or normal spinodal decomposition derived from the Cahn-Hilliard model. This is conceivably caused by the nonlinear process of lipid-film formation with drying. Thus, the unique time-dependent features reported in the present study are expected to be interpreted by the additional consideration of nonlinear kinetic process. Further theoretical studies along these lines are needed.

IV. SUMMARY

In this article, the mechanisms of the formation of phospholipid dry films under the evaporation of organic solvents are reported. Two formation kinetics for a terracelike morphology of lamellae in μm scale were found depending on the evaporation rate. Slow evaporation induces spinodal decompositionlike kinetics, while fast evaporation induces nucleation and the growth of a lamellar phase. The kinetic analysis suggests that a simple argument based on classical nucleation/spinodal behavior is insufficient to interpret the observed experimental trends. We suggest a schematic model for these formation mechanisms that can be explained in terms of the kinetic pathway in the phase diagram of a three-component system consisting of lipid, organic solvent, and water.

ACKNOWLEDGMENTS

The authors are indebted to Dr. K. Inoue at Diamond Light Source for his support with the TR-SAXS experiment at SPring-8. The SAXS experiments were performed under the approval of JASRI (Approval No. 2008A1486 and No. 2008B1410). This work was supported in part by JSPS under a Grant-in-Aid for Creative Scientific Research (Project No. 18GS0421). M.H. was supported by the JSPS (Grant No. 19-2774).

[1] E. Sackmann, Science **271**, 43 (1996).
[2] M. Tanaka and E. Sackmann, Nature (London) **437**, 656 (2005).
[3] T. Salditt, J. Phys.: Condens. Matter **17**, R287 (2005).
[4] A. D. Bangham, M. M. Standish, and J. C. Watkins, J. Mol. Biol. **13**, 238 (1965).
[5] D. D. Lasic, Biochem. J. **256**, 1 (1988).
[6] M. Hishida, H. Seto, and K. Yoshikawa, Chem. Phys. Lett. **411**, 267 (2005).
[7] M. Hishida, H. Seto, N. L. Yamada, and K. Yoshikawa, Chem. Phys. Lett. **455**, 297 (2008).
[8] M. Yanagisawa, M. Imai, T. Masui, S. Komura, and T. Ohta, Biophys. J. **92**, 115 (2007).
[9] L. Perino-Gallice, G. Fragneto, U. Mennicke, T. Salditt, and F. Rieutord, Eur. Phys. J. E **8**, 275 (2002).
[10] C. J. Brinker, Y. Lu, A. Sellinger, and H. Fan, Adv. Mater. **11**, 579 (1999).
[11] A. Gibaud, D. Grosso, B. Smarsly, A. Baptiste, J. F. Bardeau, F. Babonneau, D. A. Doshi, Z. Chen, C. Jeffrey Brinker, and C. Sanchez, J. Phys. Chem. B **107**, 6114 (2003).

[12] J. W. Cahn and J. E. Hilliard, J. Chem. Phys. **28**, 258 (1958).
[13] R. A. L. Jones, *Soft Condensed Matter* (Oxford University Press, New York, 2002).
[14] T. M. Weiss, T. Narayanan, and M. Gradzielski, Langmuir **24**, 3759 (2008).
[15] Y. Iwashita and H. Tanaka, Phys. Rev. Lett. **98**, 145703 (2007).
[16] Material safety data sheets of the chemicals, e.g., http://www.jtbaker.com/msds/englishhtml/c2915.htm and http://www.jtbaker.com/msds/englishhtml/O1694.htm
[17] W. Ostwald, Z. Phys. Chem. **37**, 385 (1901).
[18] P. W. Voorhees, J. Stat. Phys. **38**, 231 (1985).
[19] J. S. Pedersen, in *Neutrons, X-rays and Light: Scattering Methods Applied to Soft Condensed Matter*, edited by P. Linder and T. Zemb (Elsevier, Amsterdam, 2002).
[20] N. W. Ashcroft and J. Lekner, Phys. Rev. **145**, 83 (1966).
[21] Y. C. Liu, S. H. Chen, and J. S. Huang, Phys. Rev. E **54**, 1698 (1996).
[22] M. Hishida, H. Seto, P. Kaewsaiha, H. Matsuoka, and K. Yoshikawa, Colloids Surf., A **284–285**, 444 (2006).
[23] M. Rappolt, H. Amenitsh, J. Strancar, C. V. Teixeira, M. Kriechbaum, G. Pabst, M. Majerowicz, and P. Laggner, Adv. Colloid Interface Sci. **111**, 63 (2004).
[24] L. Yang and H. W. Huang, Biophys. J. **84**, 1808 (2003).
[25] M. Leaver, A. Fogden, M. Holmes, and C. Fairhurst, Langmuir **17**, 35 (2001).
[26] S. Puntambekar, M. C. Holmes, and M. S. Leaver, Liq. Cryst. **27**, 743 (2000).
[27] M. Muthukumar, Adv. Polym. Sci. **191**, 241 (2005).
[28] M. Muthukumar and P. Welch, Polymer **41**, 8833 (2000).
[29] P. Panine, E. Di Cola, M. Sztucki, and T. Narayanan, Polymer **49**, 676 (2008).
[30] Z. Xiao and Y. A. Akpalu, Polymer **48**, 5388 (2007).